

A SIMPLIFIED FAST MULTIPOLE METHOD
BASED ON STRONG RECURSIVE SKELETONIZATION

Anna Yesypenko*, Chao Chen[†], and Per-Gunnar Martinsson*

Abstract: This work introduces a kernel-independent, multilevel, adaptive algorithm for efficiently evaluating a discrete convolution kernel with a given source distribution. The method is based on linear algebraic tools such as low rank approximation and “skeleton representations” to approximate far-field interactions. While this work is related to previous linear algebraic formulations of the fast multipole method, the proposed algorithm is distinguished by relying on simpler data structures.

The proposed algorithm eliminates the need for explicit interaction lists by restructuring computations to operate exclusively on the near-neighbor list at each level of the tree, thereby simplifying both implementation and data structures. This work also introduces novel translation operators that significantly simplify the handling of adaptive point distributions. As a kernel-independent approach, it only requires evaluation of the kernel function, making it easily adaptable to a variety of kernels. By using operations on the neighbor list (of size at most 27 in 3D) rather than the interaction list (of size up to 189 in 3D), the algorithm is particularly well-suited for parallel implementation on modern hardware.

Numerical experiments on uniform and non-uniform point distributions in 2D and 3D demonstrate the effectiveness of the proposed parallel algorithm for Laplace and (low-frequency) Helmholtz kernels. The algorithm constructs a tailored skeleton representation for the given geometry during a precomputation stage. After precomputation, the fast summation achieves high efficiency on the GPU using batched linear algebra operations.

1. INTRODUCTION

We present an algorithm for evaluating a sum of the form

$$(1) \quad u_i = \sum_{j=1, i \neq j}^N G(x_i, x_j) q_j, \quad i = 1, \dots, N$$

where $\mathcal{X} = \{x_i\}_{i=1}^N$ is a given set of points in \mathbb{R}^2 or \mathbb{R}^3 , and where G is a given kernel function associated with a standard elliptic PDE of mathematical physics. For instance, G may be the fundamental solution of Laplace’s equation,

$$(2) \quad G(x_i, x_j) = \begin{cases} -\frac{1}{2\pi} \log(\|x_i - x_j\|) & x_i \neq x_j \in \mathbb{R}^2 \\ \frac{1}{4\pi\|x_i - x_j\|} & x_i \neq x_j \in \mathbb{R}^3. \end{cases}$$

The task of evaluating a sum such as (1) arises frequently in particle simulations, computational chemistry, molecular dynamics, the discretization of boundary integral equations, and many other contexts. The summation problem (1) can be viewed as a matrix-vector product

$$(3) \quad \mathbf{u} = \mathbf{A} \mathbf{q},$$

where \mathbf{A} is a dense matrix of size $N \times N$ with off-diagonal entries $A_{ij} = G(x_i, x_j)$ and zeros on the diagonal, and where $\mathbf{u} = [u_1, \dots, u_N]$ and $\mathbf{q} = [q_1, \dots, q_N]$.

*Oden Institute, University of Texas at Austin (annayesy@utexas.edu, pgm@oden.utexas.edu).

[†]Department of Mathematics, North Carolina State University (cchen49@ncsu.edu).

Evaluating (1) directly requires $\mathcal{O}(N^2)$ operations. Over the past decades, several analytic and algebraic algorithms have been proposed to evaluate (1) efficiently. For uniform particle distributions, mesh based methods leveraging the Fast Fourier Transform (FFT) achieve $\mathcal{O}(N \log N)$ complexity [11, 41, 8]. For highly adaptive point distributions, the Fast Multipole Method (FMM) is a preferred approach, offering $\mathcal{O}(N)$ complexity by operating on a hierarchical adaptive tree that partitions the given geometric points.

The original FMM used analytic expansions to efficiently approximate far-field interactions. Specifically, multipole expansions approximate the influence of source points in the far-field, while local expansions capture the effect of far-field sources on a target region. These expansions are constructed through hierarchical tree traversals: multipole expansions are computed during the upward traversal, and local expansions are computed during the downward traversal. Once the local expansions are available in the smallest target regions (leaf boxes), the result of (1) is computed by combining the contributions from the local expansions with the contributions from near neighbors, which are evaluated directly.

The FMM was first developed for the Laplace kernel [17, 37] and later extended to a wide range of kernels in computational physics [15, 14, 49], including specialized techniques for 3D applications [19, 18]. However, deriving analytic expansions for arbitrary kernels can be challenging, and implementing efficient translation operators often becomes cumbersome.

To broaden the applicability of the FMM, kernel-independent algebraic variants [48, 29, 32] were introduced. These methods exploit the algebraic property that interactions between well-separated point sets are numerically low-rank for many non-oscillatory, translation-invariant kernel functions. Using tools such as singular value decomposition (SVD) or other numerical decompositions, these techniques compress interactions without relying on analytic formulas [13, 16].

A particularly effective approach involves selecting an equivalent set of densities, or so-called skeletons, that replicate far-field interactions [48, 29, 28, 32, 7]. The skeleton points are typically precomputed algebraically for a given user tolerance and the computation of the approximate far-field interactions only involves evaluating the kernel entries, enabling portable implementations across various architectures using standard linear algebra protocols.

While kernel-independent methods simplify the handling of arbitrary kernels, they retain the same algorithmic constructs and challenges as the original analytic FMM. Specifically, translating multipole expansions to local expansions depends on efficiently traversing auxiliary data structures such as the interaction list (V-list), W-list, and X-list [47] to accumulate far-field interactions for each box. In 3D, the interaction list can contain up to 189 boxes, compared to only 27 boxes in the neighbor list. Navigating these larger data structures requires careful data management and load balancing, introducing significant implementation challenges, particularly for adaptive trees.

1.1. Contributions of the Present Work. The proposed algorithm introduces a significantly simplified kernel-independent FMM that bypasses the need for interaction lists and related auxiliary lists for adaptive trees. Instead, it relies solely on neighbor-to-neighbor interactions at each level of the tree. The key features of the method include:

- Expanded framework for outgoing and incoming expansions. The algorithm uses four types of expansions per box (two types of outgoing expansions and two types of incoming expansions), compared to two in classical FMM (multipole and local). These additional expansions help to reorganize the algorithmic structure.
- Algebraic modifications to near-neighbor computations. Rather than directly evaluating near-neighbor contributions for the smallest target boxes, the algorithm introduces algebraically modified translations. These modifications alter the recursive nature of the multi-level approach, leading to a new set of operations needed to translate outgoing expansions

to incoming expansions. These operations require traversing the near-neighbors at every level of the tree.

- Simplified translations for adaptive trees. For nonuniform trees, translations are performed on coarse neighbors (neighboring boxes at a higher level) and fine neighbors (neighboring boxes at a lower level).

Our proposed method has a minor increase in the constant prefactor compared to the traditional FMM. The prefactor costs of the classical FMM are a function of a desired accuracy and the size of the interaction list. The classical FMM traverses the interaction list to translate multipole to local expansions for every box. There are 27 and 189 boxes in the interaction list for uniform point distributions in 2D and 3D, respectively.

Our proposed algorithm in principle traverses a slightly larger list (of sizes 36 and 216 for uniform distributions in 2D and 3D, respectively) to translate outgoing expansions to incoming expansions. However, these operations are actually accumulated at the next coarsest level of the tree, requiring instead the a traversal of the neighbor list, albeit for more skeleton points in each box. A key advantage of the proposed approach is its reduced parallel overhead, as neighbor list operations require substantially less coordination and synchronization.

1.2. Context and Related Work. A common theme in recent advances in FMM-type algorithms is the improvement of practical runtime through simplified data structures, while maintaining compatibility with adaptive trees. One such example is the dual-space multilevel kernel-splitting (DMK) framework [26], which operates on adaptive trees with a multilevel method inspired by Ewald’s approach [12, 2, 39]. DMK eliminates the need for the interaction list and relies solely on the near-neighbor list, though it differs fundamentally from the present work by employing analytic rather than algebraic techniques.

Direct solvers and preconditioners for systems such as (3) — where \mathbf{A} incorporates corrections to the diagonals to ensure invertibility — have increasingly focused on simplified data structures to improve the practical performance of hierarchical matrix solvers [23, 22, 4]. Solvers using weak admissibility compress near-neighbor interactions as numerically low-rank [20, 33, 25], effectively eliminating the need for interaction lists, albeit with higher asymptotic complexity for 3D point distributions. Recent advances in direct solvers [44, 46] that build on earlier works [34, 40] construct LU or Cholesky decompositions of the FMM matrix by algebraically compressing interaction lists. This approach yields an invertible factorization that relies solely on neighbor interactions at each level of the tree.

The proposed method introduces a novel algorithmic structure that completely eliminates interaction lists from the kernel-independent FMM. By relying solely on neighbor-to-neighbor interactions, it simplifies parallel implementation on modern architectures while maintaining full compatibility with adaptive trees.

2. METHODOLOGY

In this section, the summation problem and general methodology used for the FMM are discussed. As a simple example, consider the geometry shown in Figure 1. The points are partitioned in a multi-level uniform tree \mathcal{T} , and the geometry is described by some simple terminology. Boxes on the same level are called *colleagues*. Colleagues that share an edge or corner (i.e. are adjacent) are called *neighbors*. Colleagues which are not adjacent are called *well-separated*. For a box \mathcal{B} , the set of neighbor boxes is called $\mathcal{N}(\mathcal{B})$, and the *far-field* $\mathcal{F}(\mathcal{B})$ is the set of all well-separated boxes. The *parent* $\mathcal{P}(\mathcal{B})$ of a box \mathcal{B} is the box on the next coarser level which contains \mathcal{B} . Likewise, the *children* $\mathcal{C}(\mathcal{B})$ of a box \mathcal{B} are the set of boxes whose parent is \mathcal{B} . A box \mathcal{B} without children is called a *leaf*.

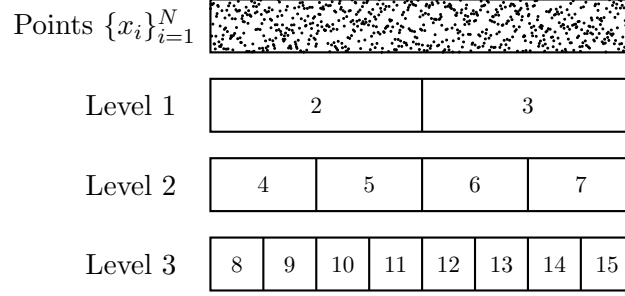


FIGURE 1. Points partitioned into multi-level tree \mathcal{T} . For a box \mathcal{B} , the set of neighbors is called $\mathcal{N}(\mathcal{B})$, and the set of well-separated boxes is called the far field $\mathcal{F}(\mathcal{B})$. As an example $\mathcal{N}(9) = \{8, 10\}$ and $\mathcal{F}(9) = \{11, \dots, 15\}$.

The kernel matrix \mathbf{A} has the following low-rank property: if two well-separated colleague boxes $\mathcal{B}_i, \mathcal{B}_j$ each contain m points, then the corresponding off-diagonal submatrix $\mathbf{A}_{\mathcal{B}_i, \mathcal{B}_j}$ satisfies

$$(4) \quad \mathbf{A}_{\mathcal{B}_i, \mathcal{B}_j} = \mathbf{E}_{\mathcal{B}_i} \tilde{\mathbf{A}} \mathbf{F}_{\mathcal{B}_j} + O(\epsilon),$$

$m \times m$ $m \times k$ $k \times k$ $k \times m$

where $\mathbf{E}_{\mathcal{B}_i}, \mathbf{F}_{\mathcal{B}_j}^* \in \mathbb{R}^{m \times k}$ are bases for the column and row spaces, respectively. In particular, the numerical rank $k \sim \mathcal{O}(\log(1/\epsilon))$ is independent of m , for a smooth non-oscillatory kernel such as the free-space Green's function for the Laplace equation (2) in 2D (see, e.g., [17]). For non-oscillatory kernels on 3D point distributions, the numerical rank k_{\max} is also independent of m but has slower decay with ϵ , in particular, $k \sim \mathcal{O}(\log(1/\epsilon)^2)$.

The low-rank property may deteriorate for oscillatory kernels, such as the Green's function for the Helmholtz equation (parameterized by the wavenumber $\kappa > 0$)

$$(5) \quad G(x_i, x_j) = \begin{cases} \frac{i}{4} H_0^{(1)}(\kappa \|x_i - x_j\|), & x_i \neq x_j \in \mathbb{R}^2 \\ \frac{1}{4} \frac{e^{i\kappa \|x_i - x_j\|}}{\|x_i - x_j\|}, & x_i \neq x_j \in \mathbb{R}^3, \end{cases}$$

where $H_0^{(1)}$ is the Hankel function of the first kind of order zero. In particular, for a box of diameter D , the numerical rank is $\mathcal{O}(\kappa D)$. To achieve log-linear complexity when the number of points scales with the wavenumber κ (maintaining a constant number of points per wavelength), specialized techniques are required. These include analytic methods (e.g., [38, 36, 6]) and algebraic approaches (e.g., [10, 3, 27]). When the wavenumber κ is fixed as the number of points m increases, the numerical rank remains independent of m . In this regime, the techniques described in this work remain applicable.



FIGURE 2. The kernel matrix \mathbf{A} corresponding to geometry in Figure 1 for the boxes on level 3 has the algebraic structure in the figure. Interactions between neighbors are full rank. The interaction between a box and its far field is low rank to accuracy ϵ , as described in (4).

The next subsections describe how the structure (4) can be used to construct a sparse factorization of \mathbf{A} that can be constructed and applied in $\mathcal{O}(N)$ time. First, Section 2.1 describes a choice of basis for (4), known as the skeleton basis, where the set of source points in a box \mathcal{B} is replaced by a subset that replicates the original effect in the far field of \mathcal{B} . Such a basis can be computed for all boxes on a single level, leading to a sparse factorization of \mathbf{A} , which is discussed in Section 2.2. Finally, Section 2.3 discusses how this process can be applied recursively on a tree \mathcal{T} to produce a multi-level algorithm that involves only neighbor calculations. The key differences between our approach and traditional FMM algorithms are highlighted as well.

2.1. Computing a skeleton basis for a single box. Consider a box \mathcal{B}_i with neighbors \mathcal{N} and far-field \mathcal{F} . Abusing notations, we also use \mathcal{B}_i , \mathcal{N} , and \mathcal{F} to denote the indices of points contained in the box, its neighbors, and its far field. Correspondingly, $\mathcal{B}_i \cup \mathcal{N} \cup \mathcal{F}$ forms a partitioning of row and column indices of the kernel matrix \mathbf{A} . For an appropriate permutation, we write \mathbf{A} as

$$(6) \quad \mathbf{A} = \begin{pmatrix} \mathbf{A}_{\mathcal{B}_i \mathcal{B}_i} & \mathbf{A}_{\mathcal{B}_i \mathcal{N}} & \mathbf{A}_{\mathcal{B}_i \mathcal{F}} \\ \mathbf{A}_{\mathcal{N} \mathcal{B}_i} & \mathbf{A}_{\mathcal{N} \mathcal{N}} & \mathbf{A}_{\mathcal{N} \mathcal{F}} \\ \mathbf{A}_{\mathcal{F} \mathcal{B}_i} & \mathbf{A}_{\mathcal{F} \mathcal{N}} & \mathbf{A}_{\mathcal{F} \mathcal{F}} \end{pmatrix}.$$

For non-oscillatory functions G , the matrices $\mathbf{A}_{\mathcal{B}_i \mathcal{F}}$ and $\mathbf{A}_{\mathcal{F} \mathcal{B}_i}$ for an arbitrary box \mathcal{B}_i can be approximated efficiently by a low-rank approximation for a prescribed accuracy ε . In this work and other works based on recursive skeletonization, we use the interpolative decomposition (ID), which selects a subset of the original columns or rows of the matrix as a basis. A (column) interpolative decomposition (ID) for a prescribed accuracy ε finds the so-called *skeleton* indices $\mathcal{S}_i \subset \mathcal{B}_i$, the *redundant* indices $\mathcal{R}_i = \mathcal{B}_i \setminus \mathcal{S}_i$, and an *interpolation matrix* $\mathbf{T}_{\mathcal{B}_i} \in \mathbb{C}^{|\mathcal{S}_i| \times |\mathcal{R}_i|}$ such that

$$\|\mathbf{A}_{\mathcal{F} \mathcal{R}_i} - \mathbf{A}_{\mathcal{F} \mathcal{S}_i} \mathbf{T}_{\mathcal{B}_i}\| \leq \varepsilon \|\mathbf{A}_{\mathcal{F} \mathcal{B}_i}\|.$$

While the strong rank-revealing QR factorization of Gu and Eisenstat [21] is the most robust method for computing an ID, this work employs the column-pivoting QR factorization as a greedy approach [7], which has better computational efficiency and behaves well in practice. For a matrix of size $m \times n$ with numerical rank k , the cost to compute an ID using the aforementioned deterministic methods is $\mathcal{O}(mnk)$, which can be further reduced to $\mathcal{O}(mn \log k + k^2 n)$ using randomized sketching [9]. Instead of compressing each block $\mathbf{A}_{\mathcal{B}_i \mathcal{F}}$ and $\mathbf{A}_{\mathcal{F} \mathcal{B}_i}$ separately, it is often convenient to conduct column ID compression of the concatenation,

$$(7) \quad \begin{pmatrix} \mathbf{A}_{\mathcal{F} \mathcal{B}_i} \\ \mathbf{A}_{\mathcal{B}_i \mathcal{F}}^* \end{pmatrix} = \begin{pmatrix} \mathbf{A}_{\mathcal{F} \mathcal{R}_i} & \mathbf{A}_{\mathcal{F} \mathcal{S}_i} \\ \mathbf{A}_{\mathcal{R}_i \mathcal{F}}^* & \mathbf{A}_{\mathcal{S}_i \mathcal{F}}^* \end{pmatrix} \approx \begin{pmatrix} \mathbf{A}_{\mathcal{F} \mathcal{S}_i} \\ \mathbf{A}_{\mathcal{S}_i \mathcal{F}}^* \end{pmatrix} \begin{pmatrix} \mathbf{T}_i & \mathbf{I} \end{pmatrix}$$

which leads to a slightly larger set of skeleton indices but makes the implementation easier. Notice that the computational cost would be $\mathcal{O}(N)$ if the full matrix in (7) is formed, which turns out to be unnecessary. Instead, the effect of the far-field points can be replicated using an artificial surface of proxy points, as is done in [48, 47, 31, 24]; see [30, Sec. 17.1] as well as [43, 42] for a detailed discussion. Instead of using the matrix in equation (7), a smaller matrix $\begin{pmatrix} \mathbf{A}_{\text{proxy } \mathcal{B}_i} \\ \mathbf{A}_{\mathcal{B}_i \text{ proxy}}^* \end{pmatrix}$ with $2 n_{\text{proxy}}$ rows is formed and compressed.

With the appropriate choice of proxy surface, the matrix $\mathbf{A}_{\text{proxy}, \mathcal{B}_i}$ provides a low-dimensional representation that captures the essential features of the column space of $\mathbf{A}_{\mathcal{F}, \mathcal{B}_i}$. Similarly, $\mathbf{A}_{\mathcal{B}_i, \text{proxy}}$ provides a low-dimensional representation of the row space of $\mathbf{A}_{\mathcal{B}_i, \mathcal{F}}$. While the two matrices have a different number of rows and columns, the proxy surface ensures that the essential relationship within these spaces is preserved for *any* point distribution in the far-field. Therefore, the indices $\mathcal{B}_i = \mathcal{R}_i \cup \mathcal{S}_i$ and interpolative matrix \mathbf{T}_i computed by forming and factorizing the smaller matrix

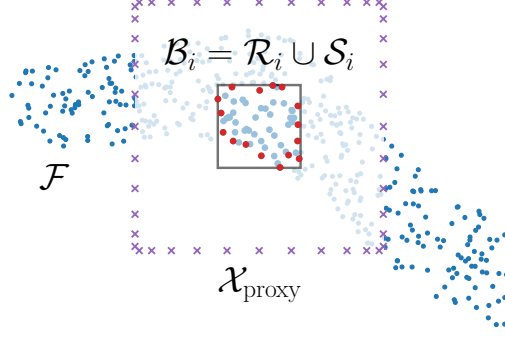


FIGURE 3. For a box \mathcal{B}_i , skeleton indices $\mathcal{S}_i \subseteq \mathcal{B}_i$ (shown in red) can be computed efficiently using a proxy surface, which are fictitious points replicating the effect of the far-field points \mathcal{F} . In our implementation of proxy surfaces, we use Chebyshev points on a box of length $2.95a$ centered at c , where a and c are the length and center of box \mathcal{B}_i , respectively.

will satisfy (7). Figure 3 shows a proxy surface for a box \mathcal{B}_i as well as the chosen subset of skeleton indices $\mathcal{S}_i \subseteq \mathcal{B}_i$.

2.2. A Single-Level Factorization. In this subsection, we use the interpolative decomposition to construct a sparse matrix factorization for the finest level of a tree-based decomposition. The section also reviews existing approaches for kernel-independent fast multipole methods and contextualizes the simplified approach proposed in this work.

Suppose that the matrix \mathbf{A} is tessellated into p blocks $\mathcal{B}_1, \dots, \mathcal{B}_p$ of size $m = N/p$ according to the finest level of \mathcal{T} . The interpolative decomposition in equation (7) can be computed for every box \mathcal{B}_i using the techniques described in Section 2.1. Using (7), the following equation holds for well-separated colleagues $\mathcal{B}_i, \mathcal{B}_j$

$$(8) \quad \mathbf{A}_{\mathcal{B}_i, \mathcal{B}_j} = \begin{pmatrix} \mathbf{A}_{\mathcal{R}_i, \mathcal{R}_j} & \mathbf{A}_{\mathcal{R}_i, \mathcal{S}_j} \\ \mathbf{A}_{\mathcal{S}_i, \mathcal{R}_j} & \mathbf{A}_{\mathcal{S}_i, \mathcal{S}_j} \end{pmatrix} \approx \begin{pmatrix} \mathbf{T}_{\mathcal{B}_i}^* \\ \mathbf{I} \end{pmatrix} \mathbf{A}_{\mathcal{S}_i, \mathcal{S}_j} \begin{pmatrix} \mathbf{T}_{\mathcal{B}_j} & \mathbf{I} \end{pmatrix} := \mathbf{E}_{\mathcal{B}_i} \mathbf{A}_{\mathcal{S}_i, \mathcal{S}_j} \mathbf{F}_{\mathcal{B}_j}.$$

$m \times k \quad k \times k \quad k \times m$

To define a single-level factorization of \mathbf{A} , it is useful to separate \mathbf{A} into near and far interactions, so that (8) can be used for the far interactions. We define $\mathbf{A}^{(\text{near})}$ and $\mathbf{A}^{(\text{far})}$ as

$$(9) \quad \left[\mathbf{A}^{(\text{near})} \right]_{i,j} := \begin{cases} \mathbf{A}_{\mathcal{B}_i, \mathcal{B}_j}, & \text{if } \mathcal{B}_i, \mathcal{B}_j \text{ are neighbors} \\ \mathbf{0}, & \text{otherwise} \end{cases}, \quad \mathbf{A}^{(\text{far})} := \mathbf{A} - \mathbf{A}^{(\text{near})}.$$

It is also useful to define the set of all skeleton indices as

$$(10) \quad \mathcal{S} = \bigcup_{i=1, \dots, p} \mathcal{S}_i, \quad \text{where } |\mathcal{S}| = pk$$

and corresponding matrices $\mathbf{A}_{\mathcal{S}, \mathcal{S}}$, which is a submatrix of \mathbf{A} , and $\mathbf{A}_{\mathcal{S}, \mathcal{S}}^{(\text{near})}$, where

$$(11) \quad \left[\mathbf{A}_{\mathcal{S}, \mathcal{S}}^{(\text{near})} \right]_{i,j} = \begin{cases} \mathbf{A}_{\mathcal{S}_i, \mathcal{S}_j}, & \text{if } \mathcal{B}_i, \mathcal{B}_j \text{ are neighbors} \\ \mathbf{0}, & \text{otherwise.} \end{cases}$$

Then $\mathbf{A}^{(\text{far})}$ can be factorized as

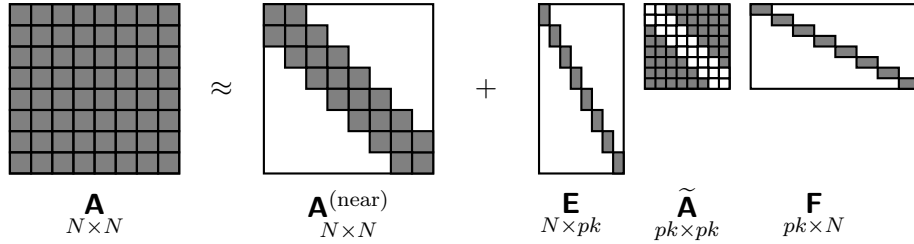
$$(12) \quad \mathbf{A}^{(\text{far})} \approx \begin{pmatrix} \mathbf{E}_{\mathcal{B}_1} & & \\ & \ddots & \\ & & \mathbf{E}_{\mathcal{B}_p} \end{pmatrix} \left(\mathbf{A}_{\mathcal{S},\mathcal{S}} - \mathbf{A}_{\mathcal{S},\mathcal{S}}^{(\text{near})} \right) \begin{pmatrix} \mathbf{F}_{\mathcal{B}_1} & & \\ & \ddots & \\ & & \mathbf{F}_{\mathcal{B}_p} \end{pmatrix} := \underbrace{\mathbf{E}}_{N \times pk} \underbrace{\tilde{\mathbf{A}}}_{pk \times pk} \underbrace{\mathbf{F}}_{pk \times N}.$$

The resulting factorization of \mathbf{A} is

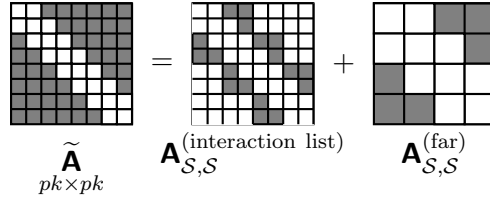
$$(13) \quad \underbrace{\mathbf{A}}_{N \times N} \approx \underbrace{\mathbf{A}^{(\text{near})}}_{N \times N} + \underbrace{\mathbf{E} \tilde{\mathbf{A}} \mathbf{F}}_{\substack{N \times pk & pk \times pk & pk \times N}}.$$

(a) sparse (b) recursive term

The sparsity patterns of the matrices in equation (13) are shown in Figure 4a for the finest level of the simple geometry in Figure 1.



(A) Sparsity pattern of $\mathbf{A} = \mathbf{A}^{(\text{near})} + \mathbf{A}^{(\text{far})}$, where $\mathbf{A}^{(\text{far})}$ is factorized using operators \mathbf{E} and \mathbf{F} . Note that $\tilde{\mathbf{A}}$ consists of sub-blocks of original kernel interactions of \mathbf{A} .



(B) Sparsity pattern of the recursive term $\tilde{\mathbf{A}}$ which can be separated into the interaction list and the far interactions on the next coarser level.

FIGURE 4. Previous approaches for the FMM separate the matrix \mathbf{A} into near and far interactions and factorize only the far-field interactions, as shown in Figure 4a. The approach can be applied recursively to $\tilde{\mathbf{A}}$, leading to the interaction list, shown in Figure 4b. For the simple geometry of Figure 1, the interaction list for a box \mathcal{B} is of size at most 3; generally, interaction list is much larger for uniform point distributions in a square (at most size 27) or in a cube (at most size 189).

To generalize from a single-level decomposition (13) to a multi-level algorithm, a similar approach can be used recursively for $\tilde{\mathbf{A}}$. The matrix can be tessellated into 4×4 blocks according to the tree decomposition on next coarser level. However, the sparsity pattern of $\tilde{\mathbf{A}}$ is significantly different from the fully-dense matrix \mathbf{A} . Instead, $\tilde{\mathbf{A}}$ can be expressed as a sum of two matrices

$$(14) \quad \tilde{\mathbf{A}} = \mathbf{A}_{\mathcal{S},\mathcal{S}}^{(\text{interaction list})} + \mathbf{A}_{\mathcal{S},\mathcal{S}}^{(\text{far})},$$

where the sparsity pattern is shown in Figure 4b. The matrix $\mathbf{A}_{\mathcal{S},\mathcal{S}}^{(\text{far})}$ consists of sub-blocks corresponding to well-separated boxes on the next coarser level. The remaining matrix $\mathbf{A}_{\mathcal{S},\mathcal{S}}^{(\text{interaction list})}$

has the so-called interaction list. Formally, box \mathcal{B}_j is in the interaction list of box \mathcal{B}_i when the boxes \mathcal{B}_i and \mathcal{B}_j are colleagues, the parents of \mathcal{B}_i and \mathcal{B}_j are neighbors, but the boxes are not themselves neighbors. In 2D, the interaction list for a box \mathcal{B} has size 27 for a fully populated tree, and in 3D, it has size 189. For the traditional FMM, additional data structures (e.g. W-list and X-list) are needed for adaptive trees. These lists, like the interaction list, require additional bookkeeping and may cause difficulty in implementing the algorithm efficiently.

2.3. A Novel Approach using Modified Neighbor Translations. In this section, we present a modified approach which leads to a multi-level algorithm which operates on much simpler data structures, requiring only the list of neighbor boxes at each level. We focus on the case of a uniform multi-level tree (e.g. Figure 1) and discuss adaptive trees in Section 3; however, adaptivity does not require much more machinery beyond what we discuss in this section.

Using the terminology of Section 2.2, we can succinctly describe our modified approach by expanding the formula (13) using (12)

$$(15) \quad \mathbf{A}_{N \times N} \approx \underbrace{\mathbf{A}_{N \times N}^{(\text{near})} - \mathbf{E}_{N \times pk} \mathbf{A}_{pk \times pk}^{(\text{near})} \mathbf{F}_{pk \times N}}_{\text{(a) sparse}} + \underbrace{\mathbf{E}_{N \times pk} \mathbf{A}_{pk \times pk} \mathbf{F}_{pk \times N}}_{\text{(b) recursive term}}.$$

We make two observations regarding (15). First, the term (15a) is sparse and involves computations between neighbors on the leaf level of the tree. Because the term $\mathbf{E} \mathbf{A}_{\mathcal{S},\mathcal{S}}^{(\text{near})} \mathbf{F}$ is explicitly subtracted in (15a), the recursive term (15b) now has different structure, compared to the recursive term (13b). Second, in (15b), $\mathbf{A}_{\mathcal{S},\mathcal{S}}$ is the kernel matrix corresponding to all pairwise interactions among skeleton points. Therefore, $\mathbf{A}_{\mathcal{S},\mathcal{S}}$ has the same low-rank property as the original matrix \mathbf{A} , and the same decomposition as in (15) can be applied recursively to $\mathbf{A}_{\mathcal{S},\mathcal{S}}$.

To describe the implementation of the matrix-vector multiply (3) using the single-level decomposition (15), we introduce some notation using the language of potential theory. With given charges \mathbf{q} , we aim to compute the potential \mathbf{u} , cf. Algorithm 1. The terminology introduced is also used in Algorithm 3 for adaptive multi-level trees.

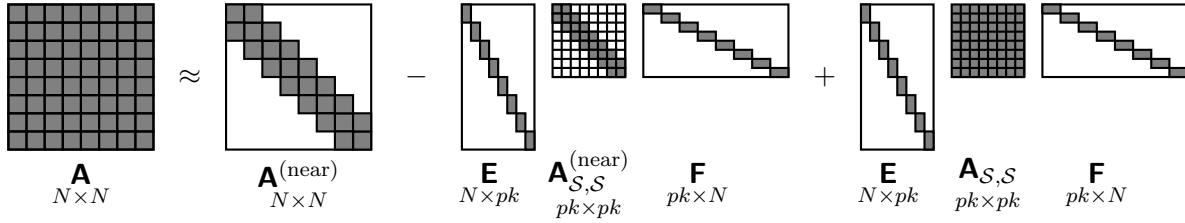
Algorithm 1 Apply using (15)

Input: Charges \mathbf{q} .

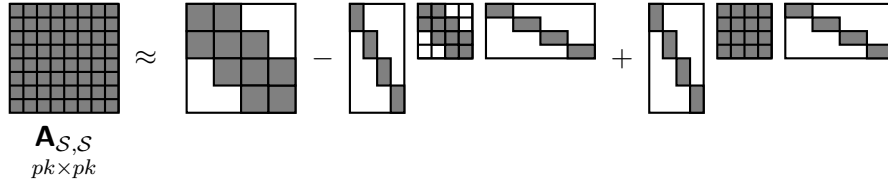
Output: Potentials \mathbf{u} .

- | | |
|--|---|
| 1: Compute $\hat{\mathbf{q}} := \mathbf{F} \mathbf{q}$. | ▷ For box \mathcal{B}_i , the outgoing representation $\hat{\mathbf{q}}_{\mathcal{S}_i} \in \mathbb{R}^k$ is an equivalent set of charges that approximates the effect of $\mathbf{q}_{\mathcal{B}_i} \in \mathbb{R}^m$ in the far field. |
| 2: Set $\mathbf{q}_{\mathcal{S}} := \hat{\mathbf{q}}$. | |
| 3: Compute $\mathbf{u}_{\mathcal{S}} := \mathbf{A}_{\mathcal{S},\mathcal{S}} \mathbf{q}_{\mathcal{S}}$. | ▷ Recursively. |
| 4: Set $\hat{\mathbf{u}} := \mathbf{u}_{\mathcal{S}}$. | |
| 5: Update $\hat{\mathbf{u}} -= \mathbf{A}_{\mathcal{S},\mathcal{S}}^{(\text{near})} \hat{\mathbf{q}}$. | ▷ For box \mathcal{B}_i , the incoming expansion $\hat{\mathbf{u}}_{\mathcal{S}_i} \in \mathbb{R}^k$ approximately captures the effect of charges from the far field. |
| 6: Compute $\mathbf{u} := \mathbf{A}^{(\text{near})} \mathbf{q} + \mathbf{E} \hat{\mathbf{u}}$. | ▷ Add contributions of neighbors. |
-

The approach involves a slightly higher constant prefactor, compared to previous approaches, because (15) essentially involves subtracting then adding a sparse matrix. The approach has benefit in ease of implementation as well as significantly less overhead to parallelizing operations over the neighbor list instead of the interaction list (e.g. 7x fewer parallel tasks in 3D for the interaction



(A) In the modified approach, the neighbor calculations involve explicitly subtracting a sparse term. This leads to a fully dense matrix in the recursive term. The matrix $\mathbf{A}_{S,S}$ is the kernel matrix corresponding to all pairwise interactions among skeleton points. Therefore, $\mathbf{A}_{S,S}$ has the same low-rank property as the original matrix \mathbf{A} if it is viewed at a coarser level.



(B) Sparsity pattern of the recursive term $\mathbf{A}_{S,S}$. Note that it is fully dense, like the original matrix \mathbf{A} . The matrix can be *coarsened* and the same approach as in (15) can be used to factorize the recursive term.

FIGURE 5. In the modified approach, we subtract an additional sparse term (15a), leading to a recursive term (15b) that has similar structure to the original matrix \mathbf{A} . A multi-level algorithm is derived by coarsening the matrix $\mathbf{A}_{S,S}$ into 4 blocks, as shown in level 2 of tree \mathcal{T} , of Figure 1. This leads to a multi-level algorithm involving *modified* neighbor interactions at every level.

list of size 189 and the neighbor list of size 27). To implement the algorithm on a multi-level tree efficiently, we also require storing *two* types of incoming and outgoing expansions since algorithm involves subtracting then summing terms; we elaborate further on these incoming and outgoing expansions in Section 3.

Briefly, we outline the scope of the remainder of the paper. In Section 3, we describe the algorithm in detail for multi-level adaptive trees, as well as describe how the algorithm can be implemented efficiently in parallel. In Section 4, we analyze the complexity to precompute the skeleton points and apply the algorithm. Finally, in section 5, we report numerical experiments on a variety of point distributions in 2D and 3D for the Laplace and low-frequency Helmholtz kernels.

3. ALGORITHM

This section describes the algorithm for adaptive quad-trees and oct-trees and extends the proposed methodology to non-uniform point distributions. While Section 2 describes a sparse factorization of \mathbf{A} , this section instead uses matrix-free notation (i.e. without explicitly forming any sparse matrices) which is more amenable to parallel implementation. Additionally, the implementation of the precomputation stage and the FMM apply are discussed.

3.1. Adaptive tree data structure. The FMM relies on a hierarchical decomposition of the points $\mathcal{X} = \{x_i\}_{i=1}^N$ into an adaptive quad-tree or oct-tree. Much of the terminology is the same as discussed earlier for the simple geometry in Figure 1 which is defined on a uniform tree. An adaptive tree can be formed using a recursive approach. First, the root box \mathcal{B}_0 which contains all the points is defined. A parameter b is also defined, for the maximum number of points a box may

have. Then \mathcal{B}_0 is split into 4 (or 8 for 3D) subdomains. Any box which is empty is pruned from the tree, and only boxes containing more than b points are subdivided recursively. The top-down construction produces a tree which is unbalanced. There may be adjacent leaf boxes that vary tremendously in their size, leading to a possibly unbounded number of neighbors for a large box adjacent to very refined box. To limit the number of interactions, adaptive trees are constrained to satisfy a 2:1 balance constraint, that is, adjacent leaf boxes must be within one level of each other. Given an unbalanced tree, additional leaves may be added in a sequential procedure that produces a balanced tree; as described in [29], this requires $\mathcal{O}(n_{\text{boxes}} \log n_{\text{boxes}})$, where n_{boxes} are the number of total boxes in the tree.

The *near-field* \mathcal{N} of box \mathcal{B} of length a and center c contains points within an area defined by a box of length $3a$ centered at c . For uniform trees, the near-field \mathcal{N} only has adjacent colleagues of \mathcal{B} , that is, boxes on the same level as \mathcal{B} which share a corner or an edge. For adaptive trees, the near-field \mathcal{N} may contain a *coarse neighbor* on a level above or a *fine neighbor* on a level below. A coarse neighbor for a box \mathcal{B} must necessarily be a leaf, which we denote \mathcal{L} ; for box \mathcal{B} to have coarse neighbor \mathcal{L} , the parent $\mathcal{P}(\mathcal{B})$ must be adjacent colleagues with \mathcal{L} , cf. Figure 6. Likewise, a leaf \mathcal{L} may have a fine neighbor \mathcal{B} . For \mathcal{T} a uniform quad-tree or oct-tree, it is obvious that no box has more than 9 and 27 neighbor boxes, respectively. For \mathcal{T} an adaptive tree with a balance constraint, the number of neighbor boxes is bounded as well.

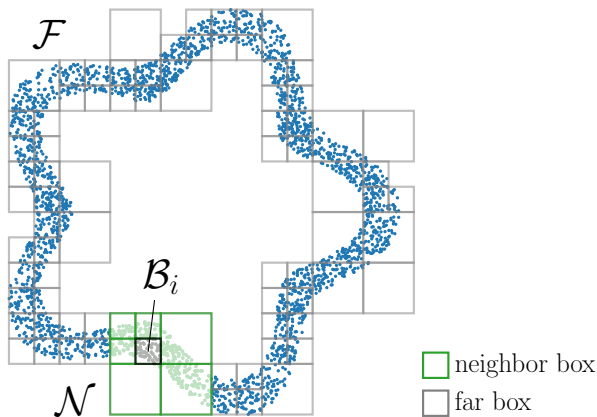


FIGURE 6. The figure shows the leaf boxes of an adaptive quadtree for a non-uniform distribution of points. The tree is adaptive, with reasonable restrictions on the adaptivity (e.g. adjacent leaf boxes are within one level of each other). For box \mathcal{B}_i with corresponding index set, we also show neighbor boxes in green and far boxes in gray. The corresponding index sets for points in the near field and far-field are \mathcal{N} and \mathcal{F} , respectively. For adaptive trees, a box \mathcal{B}_i may have a coarse neighbor on a level above or a fine neighbor on a level below.

3.2. Build stage. As described in Section 2.1, each leaf box \mathcal{B}_i can be skeletonized into redundant and skeleton indices $\mathcal{B}_i = \mathcal{R}_i \cup \mathcal{S}_i$ so that equation (7) holds. The skeleton nodes \mathcal{S}_i and interpolation matrix $\mathbf{T}_{\mathcal{B}_i}$ that satisfies (7) can be efficiently computed using a small proxy matrix. After the skeleton nodes are computed for leaf boxes, skeleton indices are computed for the remaining tree boxes (i.e. boxes with children) by traversing the tree upwards level by level. For tree boxes \mathcal{B}_i , the indices \mathcal{B}_i are set to be the union of skeleton indices of the children $\mathcal{C}(\mathcal{B}_i)$.

Algorithm 2 Strong recursive skeletonization

Input: Kernel function K and tree decomposition \mathcal{T} of points \mathcal{X} .

Output: A partition $\mathcal{B}_i = \mathcal{S}_i \cup \mathcal{R}_i$ and an interpolation matrix $\mathbf{T}_{\mathcal{B}_i}$ for each box \mathcal{B}_i .

- 1: **for** $\ell = L, L - 1, \dots, 1$ **do**
- 2: **for all** boxes \mathcal{B}_i at level ℓ **do** ▷ In parallel at each level.
- 3: **if** box \mathcal{B}_i is a leaf **then**
- 4: Determine the index vector \mathcal{B}_i from the tree decomposition \mathcal{T} .
- 5: **else**
- 6: Form the index vector \mathcal{B}_i by aggregating the skeleton indices of the children as

$$\mathcal{B}_i := \bigcup_{\mathcal{B}_j \in \mathcal{C}(\mathcal{B}_i)} \mathcal{S}_j.$$

- 7: Form a partition $\mathcal{B}_i = \mathcal{S}_i \cup \mathcal{R}_i$ and a matrix $\mathbf{T}_{\mathcal{B}_i}$ using column ID of the proxy matrix.
-

3.3. FMM apply. Sections 2.2 and 2.3 describe a sparse factorization of the kernel matrix \mathbf{A} in (3) for the finest level of a uniform tree. This section describes an efficient multi-level algorithm to compute (1) using a series of translations between incoming and outgoing expansions for each box. The modifications needed for adaptive trees are also discussed. Recall that some precomputation is required before computing (1); the skeleton indices for every box and interpolation matrices are computed in Algorithm 2 in an upward pass through the tree.

First, outgoing representations for the leaf boxes are computed as follows:

$$(16) \quad \hat{\mathbf{q}}_{\mathcal{S}_i} := (\mathbf{I} \quad \mathbf{T}_{\mathcal{L}_i}) \begin{pmatrix} \mathbf{q}_{\mathcal{S}_i} \\ \mathbf{q}_{\mathcal{R}_i} \end{pmatrix}, \quad \text{where } \mathbf{A}_{\mathcal{F}_i, \mathcal{S}_i} \hat{\mathbf{q}}_{\mathcal{S}_i} \approx \mathbf{A}_{\mathcal{F}, \mathcal{B}_i} \mathbf{q}_{\mathcal{B}_i}, \text{ for all leaves } \mathcal{L}_i.$$

In an upwards pass through the tree, outgoing representations $\mathbf{q}_{\mathcal{B}_i}, \hat{\mathbf{q}}_{\mathcal{S}_i}$ are computed for all tree boxes using formulas

$$(17) \quad \mathbf{q}_{\mathcal{B}_i} := \left[\hat{\mathbf{q}}_{\mathcal{S}_j}; \hat{\mathbf{q}}_{\mathcal{S}_{j+1}}; \dots \right] \text{ for children } \mathcal{B}_j, \mathcal{B}_{j+1}, \dots \text{ of box } \mathcal{B}_i$$

$$(18) \quad \hat{\mathbf{q}}_{\mathcal{S}_i} := (\mathbf{I} \quad \mathbf{T}_{\mathcal{B}_i}) \begin{pmatrix} \mathbf{q}_{\mathcal{S}_i} \\ \mathbf{q}_{\mathcal{R}_i} \end{pmatrix}.$$

The operation for computing $\mathbf{q}_{\mathcal{B}_i}$ in (17) involves concatenating vectors, analogous to how the index vector \mathcal{B}_i is accumulated from the children in Algorithm 2 on line 6.

At level 1 of the tree, there are at most 2^d boxes, each of which contain $k \cdot 2^d$ active indices (assuming k skeleton points per box), and the potentials due to the skeleton charges can be computed directly

$$(19) \quad \mathbf{u}_{\mathcal{B}_i} := \sum_{\mathcal{B}_j \text{ on level 1}} \mathbf{A}_{\mathcal{B}_i, \mathcal{B}_j} \mathbf{q}_{\mathcal{B}_j}, \quad \text{for all boxes } \mathcal{B}_i \text{ on level 1.}$$

In a downward pass through the tree, outgoing expansions are computed for each box \mathcal{B}_i . For each box \mathcal{B}_i at level l , the following steps are performed. First, initialize $\hat{\mathbf{u}}_{\mathcal{S}_i}$ with the parent's contributions

$$(20) \quad \hat{\mathbf{u}}_{\mathcal{S}_i} := \mathbf{u}_{\mathcal{B}_p} \text{ from parent box } p = \mathcal{P}(\mathcal{B}_i), \text{ where } \mathbf{u}_{\mathcal{B}_p} = \begin{pmatrix} \mathbf{u}_{\mathcal{S}_p} \\ \mathbf{u}_{\mathcal{R}_p} \end{pmatrix}.$$

Then, subtract contributions of skeleton indices from colleague neighbors

$$(21) \quad \hat{\mathbf{u}}_{\mathcal{S}_i} \quad - = \quad \sum_{\substack{\text{colleague} \\ \text{neighbor } \mathcal{B}_j}} \mathbf{A}_{\mathcal{S}_i, \mathcal{S}_j} \hat{\mathbf{q}}_{\mathcal{S}_j}.$$

Finally, set the outgoing representation $\mathbf{u}_{\mathcal{B}_i}$ to be the sum of contributions of box indices from colleague neighbors as well as the interpolated contribution of $\hat{\mathbf{u}}_{\mathcal{S}_i}$

$$(22) \quad \mathbf{u}_{\mathcal{B}_i} := \begin{pmatrix} \mathbf{I} \\ \mathbf{T}_{\mathcal{B}_i}^* \end{pmatrix} \hat{\mathbf{u}}_{\mathcal{S}_i} + \sum_{\substack{\text{colleague} \\ \text{neighbor } \mathcal{B}_j}} \mathbf{A}_{\mathcal{B}_i, \mathcal{B}_j} \mathbf{q}_{\mathcal{B}_j}.$$

Equation (21) subtracts the contributions of the *skeleton* indices of the neighbors and the subsequent formula (22) adds the contributions of the *box* indices of the neighbors. There is a connection to these matrix-free formulas and the earlier discussion in Section 2 that it is simple to see by referring to Figure 5a.

For adaptive trees, a box may also have a fine or coarse neighbor on the level below or above, respectively. This requires modifying the formulas (21) and (22). We again proceed level-by-level. For all boxes on a level, we initialize $\hat{\mathbf{u}}_{\mathcal{S}_i}$ as described in equation (20). Then, we subtract contributions from coarse neighbors, as well as colleague neighbors

$$(23) \quad \hat{\mathbf{u}}_{\mathcal{S}_i} \quad - = \quad \left(\sum_{\substack{\text{colleague} \\ \text{neighbor } \mathcal{B}_j}} \mathbf{A}_{\mathcal{S}_i, \mathcal{S}_j} \hat{\mathbf{q}}_{\mathcal{S}_j} + \sum_{\substack{\text{coarse} \\ \text{neighbor } \mathcal{B}_j}} \mathbf{A}_{\mathcal{S}_i, \mathcal{B}_j} \mathbf{q}_{\mathcal{B}_j} \right).$$

Finally, in addition to the terms in (22), there are contributions from fine and coarse neighbors

$$(24) \quad \mathbf{u}_{\mathcal{B}_i} := \begin{pmatrix} \mathbf{I} \\ \mathbf{T}_{\mathcal{B}_i}^* \end{pmatrix} \hat{\mathbf{u}}_{\mathcal{S}_i} + \sum_{\substack{\text{colleague} \\ \text{neighbor } \mathcal{B}_j}} \mathbf{A}_{\mathcal{B}_i, \mathcal{B}_j} \mathbf{q}_{\mathcal{B}_j} \\ + \sum_{\substack{\text{coarse} \\ \text{neighbor } \mathcal{B}_j}} \mathbf{A}_{\mathcal{B}_i, \mathcal{B}_j} \mathbf{q}_{\mathcal{B}_j} + \sum_{\substack{\text{fine} \\ \text{neighbor } \mathcal{B}_j}} \left(\mathbf{A}_{\mathcal{B}_i, \mathcal{B}_j} \mathbf{q}_{\mathcal{B}_j} - \mathbf{A}_{\mathcal{B}_i, \mathcal{S}_j} \hat{\mathbf{q}}_{\mathcal{S}_j} \right).$$

The resulting potential \mathbf{u} is obtained by assembling the potentials $\mathbf{u}_{\mathcal{L}}$ for every leaf box \mathcal{L} into a single long vector.

3.4. Parallel Implementation. To describe the efficient parallel implementation of the algorithm, we reorder the computation and introduce new notations. In particular, we define translation operators that simplify the algorithm's description. The key idea is that the order of operations can be rearranged so that the algorithm proceeds as follows:

- Upward pass. Compute the outgoing expansions for each box using the precomputed interpolation matrices $\mathbf{T}_{\mathcal{B}_i}$. These matrices transfer the outgoing expansion from child boxes to their parent boxes.
- Parallel translations between the neighbor list. Perform an embarrassingly parallel computation to determine the incoming expansion for each box. This step uses the incoming-from-outgoing translation operators between each box and its colleague neighbors. For a non-uniform tree, additional operations are required, including incoming-from-sources and targets-from-outgoing translations for both coarse and fine neighbor boxes.

- Downward pass. Compute the incoming expansions for each box. Once again, the interpolation matrices $\mathbf{T}_{\mathcal{B}_i}$ are used to transfer incoming expansions from parent boxes to their children, ultimately yielding the computed potential.

Reordering the computation in this manner ensures that the only level-to-level dependence occurs in the upward and downward passes. The translation operations, which involve evaluating kernel matrix entries, are the most computationally intensive portion of the algorithm. However, their embarrassingly parallel nature makes them well-suited for parallelization.

Table 1 summarizes the notation used to describe Algorithm 3. The parallel translation stage relies on the use of *translation operators*. For example, the incoming-from-outgoing translation converts outgoing representations $(\mathbf{q}_{\mathcal{B}_j}, \hat{\mathbf{q}}_{\mathcal{S}_j})$ in box \mathcal{B}_j to incoming representations $(\mathbf{u}_{\mathcal{B}_i}, \hat{\mathbf{u}}_{\mathcal{S}_i})$ in box \mathcal{B}_i , where boxes \mathcal{B}_i and \mathcal{B}_j are colleague neighbors.

Specifically, for a box \mathcal{B}_i with neighboring colleague \mathcal{B}_j , the operator is defined as *adding* to the outgoing expansion $\mathbf{u}_{\mathcal{B}_i}$ and *subtracting* from the outgoing expansion $\hat{\mathbf{u}}_{\mathcal{S}_i}$ by reordering equations (21a) and (22a). The operation is expressed as:

$$(\mathbf{u}_{\mathcal{B}_i}, \hat{\mathbf{u}}_{\mathcal{S}_i}) \stackrel{(\text{ifo})}{\leftarrow} (\mathbf{q}_{\mathcal{B}_j}, \hat{\mathbf{q}}_{\mathcal{S}_j}), \quad \mathbf{u}_{\mathcal{B}_i} += \mathbf{A}_{\mathcal{B}_i, \mathcal{B}_j} \mathbf{q}_{\mathcal{B}_j}, \quad \hat{\mathbf{u}}_{\mathcal{S}_i} -= \mathbf{A}_{\mathcal{S}_i, \mathcal{S}_j} \hat{\mathbf{q}}_{\mathcal{S}_j}.$$

For non-uniform trees, additional translation operators are introduced. The translation operators $\mathcal{B}_i \stackrel{(\text{ifs})}{\leftarrow} \mathcal{L}_j$, and $\mathcal{L}_i \stackrel{(\text{tfo})}{\leftarrow} \mathcal{B}_j$ are used to translate expansions between a box with a fine or coarse neighbor. These translation operators are defined in Algorithm 3.

$\mathbf{q}_{\mathcal{L}_i}$	charges at sources $\mathcal{X}_{\mathcal{L}_i}$ (given at leaves)
$\mathbf{u}_{\mathcal{L}_i}$	potentials at targets $\mathcal{X}_{\mathcal{L}_i}$ (algorithm output)
$\mathbf{q}_{\mathcal{B}_i}, \hat{\mathbf{q}}_{\mathcal{S}_i}$ $\mathbf{u}_{\mathcal{B}_i}, \hat{\mathbf{u}}_{\mathcal{S}_i}$	outgoing representations for box \mathcal{B}_i incoming representations for box \mathcal{B}_i
$\mathcal{B}_i \stackrel{(\text{ifo})}{\leftarrow} \mathcal{B}_j$	translation operator $(\mathbf{u}_{\mathcal{B}_i}, \hat{\mathbf{u}}_{\mathcal{S}_i}) \leftarrow (\mathbf{q}_{\mathcal{B}_j}, \hat{\mathbf{q}}_{\mathcal{S}_j})$ $\mathcal{B}_i \leftarrow$ colleague neighbor \mathcal{B}_j
$\mathcal{B}_i \stackrel{(\text{ifs})}{\leftarrow} \mathcal{L}_j$	translation operator $(\mathbf{u}_{\mathcal{B}_i}, \hat{\mathbf{u}}_{\mathcal{B}_i}) \leftarrow \mathbf{q}_{\mathcal{L}_j}$ $\mathcal{B}_i \leftarrow$ coarse neighbor \mathcal{L}_j
$\mathcal{L}_i \stackrel{(\text{tfo})}{\leftarrow} \mathcal{B}_j$	translation operator $\mathbf{u}_{\mathcal{L}_i} \leftarrow (\mathbf{q}_{\mathcal{B}_j}, \hat{\mathbf{q}}_{\mathcal{S}_j})$ $\mathcal{L}_i \leftarrow$ fine neighbor \mathcal{B}_j

TABLE 1. Notation used to describe the FMM apply. \mathcal{B}_i is a box in the tree (may be a leaf or not), and \mathcal{L}_i is specifically a leaf box.

Algorithm 3 FMM apply

Input: $\mathbf{q} \in \mathbb{C}^N$. For each box \mathcal{B}_i , indices $I_{\mathcal{B}_i} = I_{\mathcal{S}_i} \cup I_{\mathcal{R}_i}$, and matrix $\mathbf{T}_{\mathcal{B}_i}$.

Output: $\mathbf{u} = \mathbf{A} \mathbf{q}$.

- 1: **for all** leaf boxes \mathcal{L}_i **do**
- 2: Set $\mathbf{q}_{\mathcal{L}_i}$ to given charges.
- 3: **for all** boxes \mathcal{B}_i **do**
- 4: Set $\mathbf{u}_{\mathcal{B}_i} := \mathbf{0}$ and $\hat{\mathbf{u}}_{\mathcal{B}_i} := \mathbf{0}$.

- 5: **for** $\ell = L, L-1, \dots, 1$ **do** ▷ Upward pass.
- 6: **for all** box \mathcal{B} at level ℓ **do** ▷ In parallel at each level.
- 7: **if** box \mathcal{B}_i is a tree box **then**
- 8: Accumulate $\mathbf{q}_{\mathcal{B}_i}$ from children as

$$\mathbf{q}_{\mathcal{B}_i} := \left[\hat{\mathbf{q}}_{\mathcal{S}_j}; \hat{\mathbf{q}}_{\mathcal{S}_{j+1}}; \dots \right] \text{ for } \mathcal{B}_j, \mathcal{B}_{j+1}, \dots \in \mathcal{C}(\mathcal{B}_i).$$

- 9: Set outgoing representation

$$\hat{\mathbf{q}}_{\mathcal{S}_i} := (\mathbf{I} \quad \mathbf{T}_{\mathcal{B}_i}) \begin{pmatrix} \mathbf{q}_{\mathcal{S}_i} \\ \mathbf{q}_{\mathcal{R}_i} \end{pmatrix}$$

- 10: **for all** boxes \mathcal{B}_i with colleague neighbor \mathcal{B}_j **do** ▷ In parallel for all boxes.
- 11: Evaluate Translation $\mathcal{B}_i \xleftarrow{(\text{ifo})} \mathcal{B}_j$.

$$\mathbf{u}_{\mathcal{B}_i} += \mathbf{A}_{\mathcal{B}_i, \mathcal{B}_j} \mathbf{q}_{\mathcal{B}_j}, \quad \hat{\mathbf{u}}_{\mathcal{S}_i} -= \mathbf{A}_{\mathcal{S}_i, \mathcal{S}_j} \hat{\mathbf{q}}_{\mathcal{S}_j}$$

- 12: **for all** boxes \mathcal{B}_i with coarse neighbor \mathcal{L}_j **do** ▷ In parallel for all boxes.
- 13: Evaluate Translation $\mathcal{B}_i \xleftarrow{(\text{ifs})} \mathcal{L}_j$.

$$\mathbf{u}_{\mathcal{B}_i} += \mathbf{A}_{\mathcal{B}_i, \mathcal{L}_j} \mathbf{q}_{\mathcal{L}_j}, \quad \hat{\mathbf{u}}_{\mathcal{S}_i} -= \mathbf{A}_{\mathcal{S}_i, \mathcal{L}_j} \mathbf{q}_{\mathcal{L}_j}$$

- 14: **for all** leaves \mathcal{L}_i with fine neighbor \mathcal{B}_j **do** ▷ In parallel for all leaves.
- 15: Evaluate Translation $\mathcal{L}_i \xleftarrow{(\text{tfo})} \mathcal{B}_j$.

$$\mathbf{u}_{\mathcal{L}_i} += \mathbf{A}_{\mathcal{L}_i, \mathcal{B}_j} \mathbf{q}_{\mathcal{B}_j} - \mathbf{A}_{\mathcal{L}_i, \mathcal{S}_j} \hat{\mathbf{q}}_{\mathcal{S}_j}$$

- 16: **for all** boxes \mathcal{B}_i on level 1 **do**

- 17: Evaluate

$$\mathbf{u}_{\mathcal{B}_i} += \sum_{\mathcal{B}_j \text{ on level 1}} \mathbf{A}_{\mathcal{B}_i, \mathcal{B}_j} \mathbf{q}_{\mathcal{B}_j}.$$

- 18: **for** $\ell = 2, \dots, L$ **do** ▷ Downward pass.
- 19: **for all** boxes \mathcal{B}_i at level ℓ **do** ▷ In parallel at each level.
- 20: Add to $\hat{\mathbf{u}}_{\mathcal{S}_i}$ from relevant indices of parent box $\mathbf{u}_{\mathcal{P}(\mathcal{B}_i)}$ as

$$\hat{\mathbf{u}}_{\mathcal{S}_i} += \mathbf{u}_{\mathcal{S}_p}, \text{ where } p = \mathcal{P}(\mathcal{B}_i).$$

- 21: Add to incoming representation

$$\mathbf{u}_{\mathcal{B}_i} += \begin{pmatrix} \mathbf{I} \\ \mathbf{T}_{\mathcal{B}_i}^* \end{pmatrix} \hat{\mathbf{u}}_{\mathcal{S}_i}.$$

- 22: **for all** leaf boxes \mathcal{L}_i **do**

- 23: Set $\mathbf{u}_{\mathcal{L}_i}$ to result vector \mathbf{u} .
-

4. COMPLEXITY ANALYSIS

In this section, the computational complexity and storage costs of Algorithms 2 and 3 are analyzed. Assume that the point distribution of N particles is partitioned into a tree with at most b points in the leaf boxes, so that the total number of boxes is

$$(25) \quad n_{\text{boxes}} := n_{\text{leaf}} + n_{\text{tree}}, \quad n_{\text{leaf}} \approx N/b, \quad n_{\text{tree}} \approx \frac{1}{2^d - 1} \frac{N}{b}.$$

The number of neighbor boxes n_{neigh} depends on the point geometry; for a uniform point distribution, $n_{\text{neigh}} = 3^d$, and the quantity is bounded for balanced adaptive trees. We also define

$$(26) \quad \mathcal{N}_{\text{coarse}}(\mathcal{B}_i) := \{\mathcal{B}_j \mid \mathcal{P}(\mathcal{B}_i) \text{ and } \mathcal{P}(\mathcal{B}_j) \text{ are neighbors}\}, \quad n_{\text{coarse}} := |\mathcal{N}_{\text{coarse}}(\mathcal{B}_i)|$$

as the set of boxes such that the *parents* are neighbors. Note that this list is a superset of the interaction list and can also be defined on the next coarse level of the tree. The size of this list depends on the point distribution; it is of size at most $n_{\text{coarse}} = 6^d$ for uniform trees. We also define constants t_{kernel} and t_{flop} as the time needed for one kernel evaluation and one linear algebraic flop, respectively. We also assume that the numerical rank from ID compression is bounded by a constant k_{max} .

Precomputation Costs: For each box, we evaluate the kernel interactions between indices \mathcal{B}_i and proxy surface then compute the column ID. Assuming the accumulated skeleton indices have size at most b and the proxy surface has at most n_{proxy} points, then the total cost is

$$\begin{aligned} T_{\text{skel}} &= n_{\text{leaf}} n_{\text{proxy}} \mathcal{O}(b t_{\text{kernel}} + b k_{\text{max}} t_{\text{flop}}) \\ &+ n_{\text{tree}} n_{\text{proxy}} \mathcal{O}\left(2^d k_{\text{max}} t_{\text{kernel}} + 2^d k_{\text{max}}^2 t_{\text{flop}}\right) \\ &= \mathcal{O}(n_{\text{proxy}} (t_{\text{kernel}} + k_{\text{max}} t_{\text{flop}}) N), \end{aligned}$$

assuming that $b \geq k_{\text{max}}$. Choosing the leaf size to be at least k_{max} is a reasonable guideline to achieve competitive memory complexity as well. Under this assumption, the memory needed to store $\mathbf{T}_{\mathcal{B}_i}$ for all boxes is

$$M_{\text{proj}} = \mathcal{O}(k_{\text{max}} N).$$

Algorithm Apply: The first stage of the algorithm requires an upward pass to compute outgoing expansions $\mathbf{q}, \hat{\mathbf{q}}$ (referred to T_{of0} for the time to translate outgoing expansions). Then, computing incoming expansions $\mathbf{u}, \hat{\mathbf{u}}$ requires kernel evaluations between every box and its list of neighbors (referred to as T_{ifo} for the time for translate outgoing to incoming expansions). Finally, there is a downward pass to compute the potential at the leaves (referred to as T_{ifi} for the time to translate incoming expansions). The total time needed is

$$(27) \quad T_{\text{apply}} = T_{\text{of0}} + T_{\text{ifo}} + T_{\text{ifi}}.$$

Both the upward and downward passes require matrix-vector products with the pre-computed interpolation operators $\mathbf{T}_{\mathcal{B}_i}$, so

$$(28) \quad T_{\text{of0}} + T_{\text{ifi}} = \mathcal{O}(k_{\text{max}} t_{\text{flop}} N).$$

We now analyze the costs for translations T_{ifo} . At the leaf level, the interactions between neighbors are computed directly; this requires $n_{\text{leaf}} n_{\text{neigh}} b^2$ kernel evaluations as well as linear algebraic flops. The incoming expansions $\mathbf{u}, \hat{\mathbf{u}}$ for each box (i.e. tree or leaf box) is computed by first subtracting interactions over the skeleton indices of the neighbor list $\mathcal{N}(\mathcal{B}_i)$, then adding interactions over the skeleton indices of $\mathcal{N}_{\text{coarse}}(\mathcal{B}_i)$. The results of these computations are accumulated into $\mathbf{u}, \hat{\mathbf{u}}$ and added in the downward pass, as described in Algorithm 3. A key observation of this work is that

the traversal over $\mathcal{N}_{\text{coarse}}(\mathcal{B}_i)$ can be regrouped and described as a traversal of the neighbors *at the next coarse level*. When implementing the subtraction of neighbor interactions, one can reuse matrices that have already been formed, saving on kernel evaluation costs. The total cost is then

$$(29) \quad \begin{aligned} T_{\text{ifo}} &= n_{\text{leaf}} n_{\text{neigh}} b^2 (t_{\text{kernel}} + t_{\text{flop}}) \\ &\quad + n_{\text{boxes}} (n_{\text{coarse}} k_{\text{max}}^2 (t_{\text{kernel}} + t_{\text{flop}}) + n_{\text{neigh}} k_{\text{max}}^2 t_{\text{flop}}) \\ T_{\text{apply}} &= \mathcal{O} ((b n_{\text{neigh}} + k_{\text{max}} n_{\text{coarse}}) (t_{\text{kernel}} + t_{\text{flop}}) N). \end{aligned}$$

The resulting asymptotic costs are slightly higher than the traditional FMM, however, by grouping $\mathcal{N}_{\text{coarse}}(\mathcal{B}_i)$ on the coarser level of the tree, the algorithm traverses the neighbor list at every level. This leads to fewer parallel tasks (e.g. smaller overhead cost) and substantial benefits in the ease of implementing the algorithm.

5. NUMERICAL RESULTS

This section demonstrates the performance of a parallel implementation of the algorithm for both uniform and non-uniform point distributions in 2D and 3D. The implementation consists of a precomputation stage on the CPU. Once precomputation is complete, the algorithm rapidly computes the potential (1) on the GPU.

5.1. Precomputation Stage. The precomputation stage determines skeleton indices and computes interpolation matrices $\mathbf{T}_{\mathcal{B}_i}$, which translate incoming and outgoing expansions between child and parent boxes. This phase is performed on the CPU in double precision (or complex double precision for Helmholtz kernels), using OpenMP for parallelization across boxes at each tree level. The skeleton rank k adaptively chosen for each box based on a user-specified tolerance, with the maximum rank across all boxes denoted as k_{max} .

Because the apply-stage uses single precision, these are stored in single precision (or complex single precision for Helmholtz kernels). We report precomputation metrics T_{skel} as the time required to compute the skeleton indices and interpolation matrices, as well as M_{proj} , which is the memory needed to store all interpolation matrices $\mathbf{T}_{\mathcal{B}_i}$.

The method operates on an adaptive tree \mathcal{T} that satisfies the 2:1 balance constraint, as described in Section 3.1. Tree construction begins with a downward traversal to create an unbalanced tree where each leaf box contains at most b points. The tree is then balanced by introducing additional leaf nodes using a sequential algorithm. Geometric lookups are handled efficiently using Morton codes. The time to partition and balance the tree is denoted as T_{tree} .

5.2. GPU Implementation of Apply Stage. Once the precomputation is complete, the apply stage computes the potential (1) using the GPU for computationally intensive tasks. The computation is conducted in single precision (or complex single precision for the Helmholtz kernels).

The upward pass, which computes outgoing expansions, relies on matrix-vector products with the precomputed interpolation matrices $\mathbf{T}_{\mathcal{B}_i}$. To reduce memory overhead, the interpolation matrices are stored on the CPU, and the upward pass is executed on the CPU. The computed outgoing expansions are then transferred to the GPU.

The translation operators, which convert outgoing expansions to incoming expansions, are the most computationally intensive portion of the FMM apply stage. These operations involve kernel evaluations and matrix-vector products between sub-blocks of the kernel matrices $\mathbf{A}_{\mathcal{B}_i, \mathcal{B}_j}$. To optimize GPU performance, we use the following strategies:

- **Batching.** Translation operators are grouped into large batches of tens of thousands of submatrices to exploit GPU parallelism efficiently.

- Zero padding. Adaptive ranks are padded with zeros to ensure uniform vector lengths, enabling efficient batched operations.
- On-the-fly row generation. Instead of forming the submatrices $\mathbf{A}_{\mathcal{B}_i, \mathcal{B}_j}$ explicitly (which incurs significant memory overheads), rows are generated on-the-fly in batches and applied to the vector sequentially, row by row. This approach minimizes memory overheads and is highly cache-optimized, especially when processing over large batch sizes of grouped submatrices.

Once the outgoing expansions are computed, they are transferred back to the CPU for the downward pass, which propagates incoming expansions from the parents to the children using the interpolation matrices. The result is accumulated values $\mathbf{u}_{\mathcal{L}_i}$ stored in the leaf boxes. The time needed to compute the potential using Algorithm 3 is reported as T_{apply} , as well as relerr , the maximum relative error, evaluated on a subset of points. Table 2 summarizes the notation used for reporting the results.

N	number of points
b	leaf size of tree
k_{max}	maximum skeleton rank
T_{tree}	time to partition and balance tree
T_{skel}	time for Algorithm 2
M_{proj}	memory needed for $\mathbf{T}_{\mathcal{B}}$ for all boxes
T_{apply}	time for Algorithm 3
relerr	maximum relative error (evaluated on a subset of points)

TABLE 2. Notation for reported numerical results.

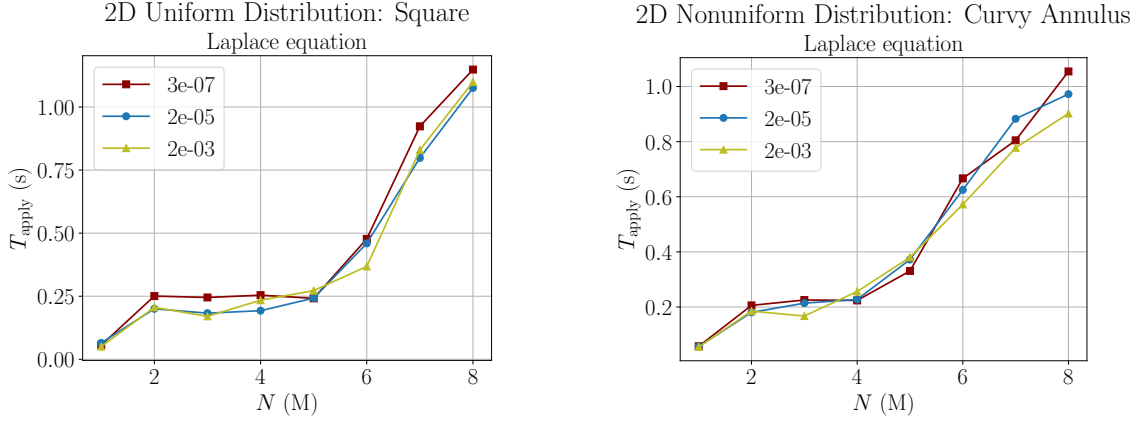
5.3. Overview of Implementation. The code is implemented in `Python`. The pre-processing stage uses the packages `numpy` and `scipy` with parallelization via OpenMP on the CPU.

The GPU implementation of the FMM apply stage uses `PyTorch`. Most of the computation time is spent on evaluating and applying kernel matrices. To optimize these operations, the `Pykeops` package [5] is employed. `Pykeops` generates highly optimized, compiled CUDA implementations of batched matrix-vector multiplications with kernel matrices, ensuring minimal memory overhead. The Hankel function $H_0^{(1)}$ is not available in `Pykeops`, and the translation operators for the 2D Helmholtz kernel are implemented (less efficiently) in `Cupy`.

The numerical experiments were conducted on a workstation equipped with an Intel Xeon Gold 6326 CPU (2.9 GHz, 16 cores) with 250 GB of RAM as well as an NVIDIA A100 GPU with 80 GB of RAM. The code is publicly available at [45] with tutorials for implementing the algorithm.

5.4. 2D Experiments. Figure 7 presents results for the Laplace kernel, while Figure 8 reports results for the 2D Helmholtz kernel with $\kappa = 100$. Both figures illustrate the performance of the method across a range of user-specified tolerances. For 2D point distributions, the skeleton rank scales approximately as $k_{\text{max}} \sim \log(1/\epsilon)$ for the Laplace equation.

The method shows strong performance on the GPU, with the runtime T_{apply} increasing only slightly as the user tolerance ϵ is refined. However, for small sub-matrix sizes, there may be overheads associated with GPU usage. The runtime remains nearly constant in the pre-asymptotic range before transitioning to a linear scaling regime.



(A) 2D Laplace kernel for points in square.

(B) 2D Laplace kernel for points in curvy annulus.

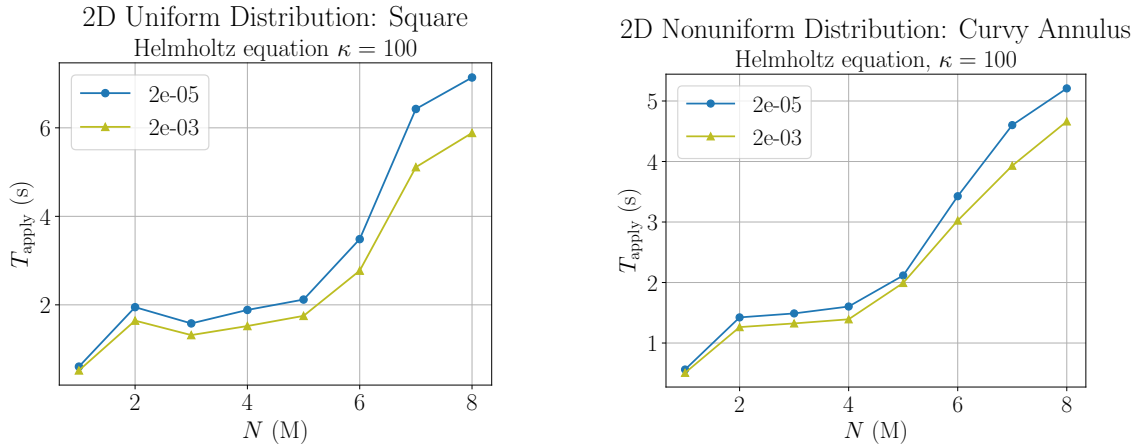
N	b	k_{\max}	T_{tree}	T_{skel}	M_{proj}	T_{apply}	relerr
1 M	100	10		4.0 s	0.1 GB	50 ms	1.31e-03
		18	1.8 s	3.0 s	0.2 GB	65 ms	7.32e-06
		28		3.4 s	0.2 GB	56 ms	2.26e-07
8 M	100	10		69.2 s	1.5 GB	1099 ms	9.36e-04
		18	29.4 s	56.3 s	2.6 GB	1076 ms	8.70e-06
		28		56.5 s	3.8 GB	1148 ms	3.69e-07

(C) 2D Laplace kernel for points in square.

N	b	k_{\max}	T_{tree}	T_{skel}	M_{proj}	T_{apply}	relerr
1 M	100	9		3.5 s	0.1 GB	55 ms	1.12e-03
		17	4.5 s	3.4 s	0.2 GB	57 ms	1.96e-05
		26		3.4 s	0.3 GB	58 ms	4.45e-07
8 M	100	9		55.6 s	1.4 GB	902 ms	1.54e-03
		17	52.2 s	54.3 s	2.5 GB	972 ms	1.01e-05
		27		41.2 s	3.6 GB	1055 ms	3.89e-07

(D) 2D Laplace kernel for points in curvy annulus.

FIGURE 7. The performance for the Laplace 2D kernel (2) is demonstrated for two point distributions. Figure 7a reports T_{apply} for a random distribution of points in $[0, 1]^2$ with additional data reported in Table 7c. Similarly, Figure 7b and Table 7d report results for points in a wiggly torus, as shown in Figure 6.



(A) 2D Helmholtz kernel for points in square. (B) 2D Helmholtz kernel for points in curly annulus.

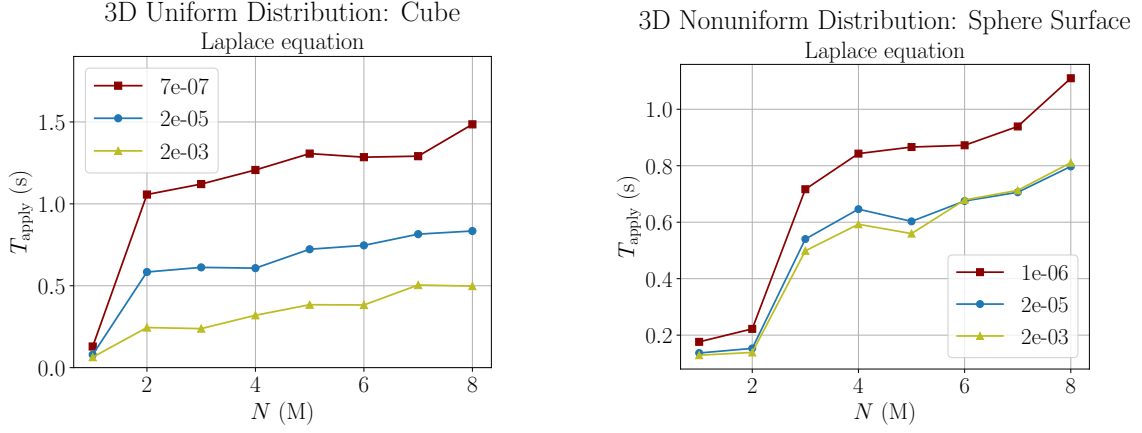
N	b	k_{\max}	T_{tree}	T_{skel}	M_{proj}	T_{apply}	relerr
1 M	100	32	2.0 s	3.3 s	0.3 GB	518 ms	8.19e-04
		39		4.4 s	0.5 GB	604 ms	7.73e-06
8 M	100	32	30.1 s	32.3 s	5.1 GB	5884 ms	2.25e-03
		40		37.8 s	8.3 GB	7137 ms	7.30e-06

(C) 2D Helmholtz kernel ($\kappa = 100$) for points in square.

N	b	k_{\max}	T_{tree}	T_{skel}	M_{proj}	T_{apply}	relerr
1 M	100	29	4.4 s	3.1 s	0.3 GB	508 ms	1.77e-03
		37		3.6 s	0.5 GB	562 ms	1.14e-05
8 M	100	30	51.6 s	32.4 s	3.8 GB	4662 ms	1.27e-03
		36		34.9 s	6.6 GB	5208 ms	6.15e-06

(D) 2D Helmholtz kernel ($\kappa = 100$) for points in curly annulus.

FIGURE 8. The performance for the Helmholtz 2D kernel (5) for $\kappa = 100$ is demonstrated for two point distributions. Figure 8a reports T_{apply} for a random distribution of points in $[0, 1]^2$ with additional data reported in Table 8c. Similarly, Figure 8b and Table 8d report results for points in a wiggly torus. The use of single-precision with a complex-valued kernel leads to some loss of accuracy for the strictest compression tolerance, we are limited to approximately 5 digits of accuracy, instead of 7, as for the 2D Laplace kernel, in Figure 7.



(A) 3D Laplace kernel for points in cube.

(B) 3D Laplace kernel for points on sphere surface.

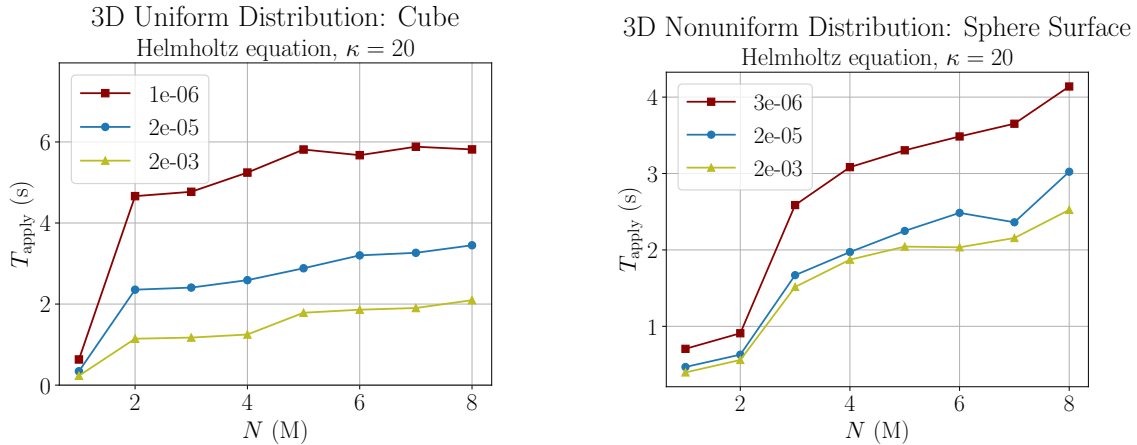
N	b	k_{\max}	T_{tree}	T_{skel}	M_{proj}	T_{apply}	relerr
1 M	320	30		2.8 s	0.2 GB	64 ms	1.34e-03
		97	1.2 s	6.1 s	0.5 GB	79 ms	1.29e-05
		181		14.9 s	1.0 GB	129 ms	3.78e-07
8 M	320	31		13.0 s	1.4 GB	498 ms	1.76e-03
		101	14.5 s	27.6 s	4.4 GB	834 ms	1.12e-05
		190		60.7 s	9.2 GB	1485 ms	7.51e-07

(C) 3D Laplace kernel for points in cube.

N	b	k_{\max}	T_{tree}	T_{skel}	M_{proj}	T_{apply}	relerr
1 M	200	17		3.9 s	0.3 GB	129 ms	2.64e-03
		41	2.9 s	5.0 s	0.7 GB	137 ms	1.43e-05
		75		7.2 s	1.5 GB	176 ms	6.62e-07
8 M	200	17		17.8 s	1.7 GB	811 ms	1.32e-03
		41	39.0 s	22.4 s	4.0 GB	797 ms	1.42e-05
		75		30.2 s	8.3 GB	1110 ms	1.26e-06

(D) 3D Laplace kernel for points on sphere surface.

FIGURE 9. The performance for the Laplace 3D kernel (2) is demonstrated for two point distributions. Figure 9a reports T_{apply} for a random distribution of points in $[0, 1]^3$ with additional data reported in Table 9c. Similarly, Figure 9b and Table 9d report results for points on the surface of the sphere.



(A) 3D Helmholtz kernel for points in cube. (B) 3D Helmholtz kernel for points on sphere surface.

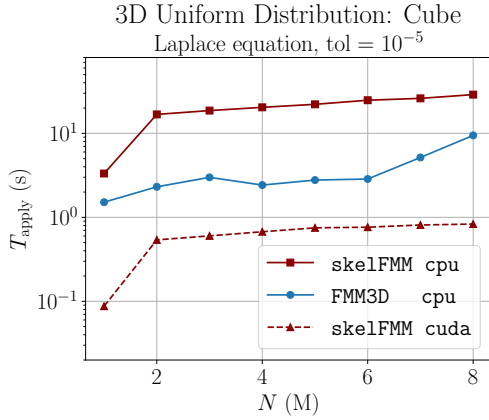
N	b	k_{\max}	T_{tree}	T_{skel}	M_{proj}	T_{apply}	relerr
1 M	320	56	1.1 s	5.9 s	0.5 GB	231 ms	9.56e-04
		127		13.3 s	1.3 GB	342 ms	5.04e-06
		211		28.8 s	2.5 GB	633 ms	2.43e-06
8 M	320	58	14.6 s	24.9 s	3.4 GB	2096 ms	9.62e-04
		133		53.9 s	10.9 GB	3450 ms	1.11e-05
		225		133.8 s	22.5 GB	5816 ms	1.60e-06

(C) 3D Helmholtz kernel ($\kappa = 20$) for points in cube.

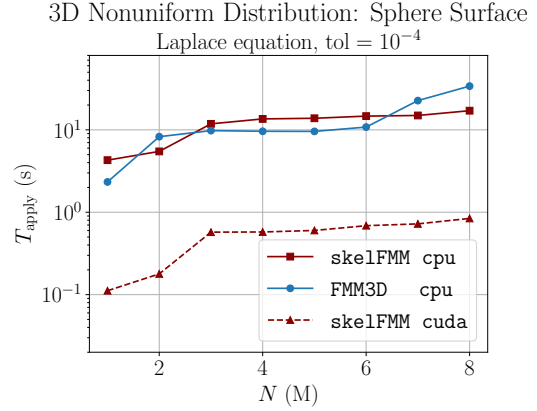
N	b	k_{\max}	T_{tree}	T_{skel}	M_{proj}	T_{apply}	relerr
1 M	200	30	3.0 s	5.6 s	0.7 GB	397 ms	1.04e-03
		59		7.7 s	1.7 GB	468 ms	5.93e-06
		96		12.1 s	3.4 GB	706 ms	4.12e-06
8 M	200	29	39.3 s	27.0 s	3.9 GB	2524 ms	1.50e-03
		60		35.0 s	9.1 GB	3023 ms	1.05e-05
		96		51.9 s	19.0 GB	4139 ms	3.40e-06

(D) 3D Helmholtz kernel ($\kappa = 20$) for points on sphere surface.

FIGURE 10. The performance for the Helmholtz 3D kernel (5) for $\kappa = 20$ is demonstrated for two point distributions. Figure 10a reports T_{apply} for a random distribution of points in $[0, 1]^3$ with additional data reported in Table 10c. Similarly, Figure 10b and Table 10d report results for points on the surface of a sphere.



(A) Laplace kernel for points in a cube.



(B) Laplace kernel for points on sphere surface.

	N	b	T_{apply}	relerr
skelFMM cpu		320	3.3 s	1.28e-05
FMM3D cpu	1 M	40	1.5 s	2.65e-05
skelFMM cuda		320	87 ms	1.28e-05
skelFMM cpu		320	28.9 s	1.19e-05
FMM3D cpu	8 M	40	9.4 s	2.44e-05
skelFMM cuda		320	831 ms	1.19e-05

(C) Laplace kernel for points in a cube.

	N	b	T_{apply}	relerr
skelFMM cpu		320	4.2 s	9.67e-05
FMM3D cpu	1 M	40	2.3 s	1.35e-04
skelFMM cuda		320	112 ms	9.56e-05
skelFMM cpu		320	17.0 s	1.10e-04
FMM3D cpu	8 M	40	33.9 s	8.19e-05
skelFMM cuda		320	841 ms	8.30e-05

(D) Laplace kernel for points on sphere surface.

FIGURE 11. The figure compares the performance of `skelFMM`, run on the CPU (using double precision) and GPU (using single precision), to `FMM3D`, a well-established FMM package implemented in Fortran (using double precision). Only the application time, T_{apply} , is reported, noting that `FMM3D` includes a more efficient precomputation stage.

Operation	Sphere Laplace, $N = 4$ M, $\text{tol} = 10^{-4}$				Cube Laplace, $N = 4$ M, $\text{tol} = 10^{-5}$			
	skelFMM cuda		skelFMM cpu		skelFMM cuda		skelFMM cpu	
upward pass	60 ms	10.3 %	93 ms	0.7 %	125 ms	18.7 %	120 ms	0.6 %
add to $\mathbf{u}_{\mathcal{B}}$ (leaf)	132 ms	22.8 %	6.0 s	44.4 %	106 ms	15.8 %	8.9 s	43.6 %
add to $\mathbf{u}_{\mathcal{B}}$ (tree)	104 ms	17.9 %	4.7 s	34.8 %	110 ms	16.4 %	6.5 s	31.9 %
subtract (ifo)	89 ms	15.3 %	1.3 s	9.6 %	105 ms	15.7 %	4.6 s	22.5 %
subtract (tfi,ifs)	29 ms	5.0 %	800 ms	5.9 %	0 ms	0.0 %	0 ms	0.0 %
downward pass	115 ms	19.8 %	150 ms	1.1 %	213 ms	31.8 %	326 ms	1.6 %
Total time	580 ms		13.5 s		670 ms		20.4 s	

TABLE 3. Detailed breakdown of execution times (in milliseconds or seconds) and their percentage contributions for major operations in the `skelFMM` algorithm. The analysis highlights the performance benefits of GPU acceleration and identifies dominant operations, such as adding to $\mathbf{u}_{\mathcal{B}}$ for tree and leaf boxes, as well as suggests possible room for improvement for more optimized implementations.

5.5. 3D Experiments. Figures 9 and 10 present results for the Laplace and Helmholtz kernels $\kappa = 20$, respectively, for 3D point distributions. For points distributed within 3D volumes, the skeleton ranks k_{\max} increase significantly as a function of the tolerance ϵ , approximately scaling as $k \sim (\log(1/\epsilon))^2$. The oct-tree data structure also leads to larger accumulated tree box sizes, increasing from $4k$ in 2D to $8k$ in 3D. Despite the increased computational demands due to higher ranks, larger sub-block sizes, and a greater number of near neighbors in 3D, the runtime for the 3D Laplace equation remains competitive. This efficiency is largely due to the effective GPU handling of translation operators. Additionally, the larger matrix sub-block sizes in 3D benefit from GPU parallelism, mitigating the overheads typically observed with smaller sub-matrix sizes in 2D.

Selecting skeleton points as a subset of the original points is particularly effective for representing surface distributions. As shown in Table 9d, this method achieves high accuracy with relatively low skeleton ranks, especially when compared to volumetric distributions (Table 9c). The cost of computing a skeleton representation tailored to the geometry can be amortized across multiple right-hand sides, making it particularly useful for the iterative solution of discretized boundary integral equations.

5.6. Performance Comparison. We compare the performance of FMM3D, a widely used CPU implementation of the fast multipole method, to `skelFMM` in its CPU and GPU variants (Figure 11). Table 3 provides a detailed breakdown of the time spent in various parts of the `skelFMM` algorithm. FMM3D [1] employs analytic expansions and advanced techniques such as directional groupings and diagonal translations [18, 35], making it a good benchmark for assessing the performance of alternative FMM implementations.

For uniform distributions in the volume, the results indicate room for improving `skelFMM`'s performance, as FMM3D incorporates advanced techniques, such as directional groupings, to more efficiently process the interaction list. In contrast, for adaptive distributions, such as on the sphere surface, the performance gap between the CPU implementations of the two codes is much narrower, indicating effective handling of non-uniform point distributions by `skelFMM` and benefits from `skelFMM`'s tailored skeleton representation.

The results clearly demonstrate the substantial performance improvements achieved through GPU acceleration. On the CPU, processing large subblock sizes incurs significant computational overhead, whereas the GPU efficiently manages many thousands of subblocks using batched operations. Notably, computational bottlenecks present in the CPU implementation of `skelFMM` are largely mitigated on the GPU. `skelFMM cuda` achieves significant speedups, outperforming `skelFMM cpu` by 34x for the cube and 20x for the sphere. `skelFMM cuda` also outperforms FMM3D by 11x for the cube and 40x for the sphere, though these results should be interpreted with caution, as they reflect the differences in CPU and GPU architectures rather than a purely algorithmic advantage.

6. CONCLUSIONS

This work introduces a novel kernel-independent algorithm for the fast multipole method (FMM). Similar to many other kernel-independent methods, analytical expansions are replaced by a chosen set of ‘skeleton’ points, which replicate the effect of the original source points in the far field.

A key contribution of this work is the elimination of interaction lists and auxiliary data structures from the kernel-independent FMM, while retaining compatibility with adaptive trees. Instead, the proposed algorithm describes novel incoming-from-outgoing translation operators involving only the neighbor list at each level, resulting in much simpler data structures. Although this adjustment introduces a slight increase in computational complexity, it significantly streamlines the computation, reducing parallel overheads and enhancing the overall efficiency of the algorithm.

Numerical results confirm the effectiveness of the GPU implementation for the Laplace and Helmholtz kernels across a range of tolerances and problem sizes. The GPU-accelerated `skelFMM cuda` variant delivers substantial speedups compared to its CPU counterpart and exhibits competitive performance with benchmark code `FMM3D`, particularly for adaptive point distributions.

This framework opens exciting opportunities for further development. For volume distributions or scenarios requiring faster precomputation, adopting a uniform skeleton basis across boxes, as explored in [29, 28], could further enhance efficiency. FFT-based accelerations and directional groupings could also optimize translation operations, particularly for high-accuracy 3D computations. Additionally, the simplicity of the neighbor-list-based approach positions this method as a strong candidate for extensions into efficient direct solvers or preconditioners for integral equations, where simpler data structures can lead to significant computational benefits.

Acknowledgments. The work reported was supported by the Office of Naval Research (N00014-18-1-2354), by the National Science Foundation (DMS-1952735, DMS-2012606, and DMS-2313434), and by the Department of Energy ASCR (DE-SC0022251). We thank Umberto Villa for access to computing resources.

REFERENCES

- [1] T. Askham et al. *Flatiron Institute Fast Multipole Libraries for the Laplace and Helmholtz kernels in three dimensions*. 2021. URL: <https://github.com/flatironinstitute/FMM3D>.
- [2] Joar Bagge and Anna-Karin Tornberg. “Fast Ewald summation for Stokes flow with arbitrary periodicity”. In: *Journal of Computational Physics* 493 (2023), p. 112473.
- [3] Austin R Benson et al. “A parallel directional fast multipole method”. In: *SIAM Journal on Scientific Computing* 36.4 (2014), pp. C335–C352.
- [4] Steffen Börm, Lars Grasedyck, and Wolfgang Hackbusch. “Introduction to hierarchical matrices with applications”. In: *Engineering analysis with boundary elements* 27.5 (2003), pp. 405–422.
- [5] Benjamin Charlier et al. “Kernel Operations on the GPU, with Autodiff, without Memory Overflows”. In: *Journal of Machine Learning Research* 22.74 (2021), pp. 1–6. URL: <http://jmlr.org/papers/v22/20-275.html>.
- [6] Hongwei Cheng et al. “A wideband fast multipole method for the Helmholtz equation in three dimensions”. In: *Journal of Computational Physics* 216.1 (2006), pp. 300–325.
- [7] Hongwei Cheng et al. “On the compression of low rank matrices”. In: *SIAM Journal on Scientific Computing* 26.4 (2005), pp. 1389–1404.
- [8] Tom Darden, Darrin York, and Lee Pedersen. “Particle mesh Ewald: An $N \log(N)$ method for Ewald sums in large systems”. In: *The Journal of chemical physics* 98.12 (1993), pp. 10089–10092.
- [9] Yijun Dong and Per-Gunnar Martinsson. “Simpler is better: a comparative study of randomized pivoting algorithms for CUR and interpolative decompositions”. In: *Advances in Computational Mathematics* 49.4 (2023), p. 66.
- [10] Björn Engquist and Lexing Ying. “Fast directional multilevel algorithms for oscillatory kernels”. In: *SIAM Journal on Scientific Computing* 29.4 (2007), pp. 1710–1737.
- [11] Ulrich Essmann et al. “A smooth particle mesh Ewald method”. In: *The Journal of chemical physics* 103.19 (1995), pp. 8577–8593.
- [12] Paul P Ewald. “Die Berechnung optischer und elektrostatischer Gitterpotentiale”. In: *Annalen der physik* 369.3 (1921), pp. 253–287.

- [13] William Fong and Eric Darve. “The black-box fast multipole method”. In: *Journal of Computational Physics* 228.23 (2009), pp. 8712–8725.
- [14] Yuhong Fu and Gregory J Rodin. “Fast solution method for three-dimensional Stokesian many-particle problems”. In: *International Journal for Numerical Methods in Biomedical Engineering* 16.2 (2000), pp. 145–149.
- [15] Yuhong Fu et al. “A fast solution method for three-dimensional many-particle problems of linear elasticity”. In: *International Journal for Numerical Methods in Engineering* 42.7 (1998), pp. 1215–1229.
- [16] Zydrunas Gimbutas and Vladimir Rokhlin. “A generalized fast multipole method for nonoscillatory kernels”. In: *SIAM Journal on Scientific Computing* 24.3 (2003), pp. 796–817.
- [17] Leslie Greengard and Vladimir Rokhlin. “A fast algorithm for particle simulations”. In: *Journal of computational physics* 73.2 (1987), pp. 325–348.
- [18] Leslie Greengard and Vladimir Rokhlin. “A new version of the fast multipole method for the Laplace equation in three dimensions”. In: *Acta numerica* 6 (1997), pp. 229–269.
- [19] Leslie Greengard and Vladimir Rokhlin. *A new version of the fast multipole method for the Laplace equation in three dimensions*. Tech. rep. YALE UNIV NEW HAVEN CT DEPT OF COMPUTER SCIENCE, 1996.
- [20] Leslie Greengard et al. “Fast direct solvers for integral equations in complex three-dimensional domains”. In: *Acta Numerica* 18 (2009), pp. 243–275.
- [21] Ming Gu and Stanley C Eisenstat. “Efficient algorithms for computing a strong rank-revealing QR factorization”. In: *SIAM Journal on Scientific Computing* 17.4 (1996), pp. 848–869.
- [22] Wolfgang Hackbusch. “A sparse matrix arithmetic based on-matrices. Part I: Introduction to-matrices”. In: *Computing* 62.2 (1999), pp. 89–108.
- [23] Wolfgang Hackbusch et al. *Hierarchical matrices: algorithms and analysis*. Vol. 49. Springer, 2015.
- [24] Kenneth L Ho and Lexing Ying. “Hierarchical interpolative factorization for elliptic operators: integral equations”. In: *Comm. Pure Appl. Math* 69.7 (2016), pp. 1314–1353.
- [25] Kenneth L. Ho and Leslie Greengard. “A Fast Direct Solver for Structured Linear Systems by Recursive Skeletonization”. In: *SIAM Journal on Scientific Computing* 34.5 (2012), A2507–A2532.
- [26] Shidong Jiang and Leslie Greengard. “A dual-space multilevel kernel-splitting framework for discrete and continuous convolution”. In: *Communications on Pure and Applied Mathematics* (2023).
- [27] Yingzhou Li et al. “Butterfly factorization”. In: *Multiscale Modeling & Simulation* 13.2 (2015), pp. 714–732.
- [28] Dhairya Malhotra and George Biros. “Algorithm 967: A distributed-memory fast multipole method for volume potentials”. In: *ACM Transactions on Mathematical Software (TOMS)* 43.2 (2016), pp. 1–27.
- [29] Dhairya Malhotra and George Biros. “PVFMM: A parallel kernel independent FMM for particle and volume potentials”. In: *Communications in Computational Physics* 18.3 (2015), pp. 808–830.
- [30] Per-Gunnar Martinsson. *Fast direct solvers for elliptic PDEs*. SIAM, 2019.
- [31] Per-Gunnar Martinsson and Vladimir Rokhlin. “A fast direct solver for boundary integral equations in two dimensions”. In: *Journal of Computational Physics* 205.1 (2005), pp. 1–23.
- [32] Per-Gunnar Martinsson and Vladimir Rokhlin. “An accelerated kernel-independent fast multipole method in one dimension”. In: *SIAM Journal on Scientific Computing* 29.3 (2007), pp. 1160–1178.

- [33] Eric Michielssen, Amir Boag, and Weng Cho Chew. “Scattering from elongated objects: Direct solution in $\mathcal{O}(n \log^2 n)$ operations”. In: *IEEE Proceedings-Microwaves, Antennas and Propagation* 143.4 (1996), pp. 277–283.
- [34] Victor Minden et al. “A recursive skeletonization factorization based on strong admissibility”. In: *Multiscale Modeling & Simulation* 15.2 (2017), pp. 768–796.
- [35] Vladimir Rokhlin. *Diagonal forms of translation operators for Helmholtz equation in three dimensions*. Tech. rep. DTIC Document, 1992.
- [36] Vladimir Rokhlin. “Diagonal forms of translation operators for the Helmholtz equation in three dimensions”. In: *Applied and computational harmonic analysis* 1.1 (1993), pp. 82–93.
- [37] Vladimir Rokhlin. “Rapid solution of integral equations of classical potential theory”. In: *Journal of computational physics* 60.2 (1985), pp. 187–207.
- [38] Vladimir Rokhlin. “Rapid solution of integral equations of scattering theory in two dimensions”. In: *Journal of Computational physics* 86.2 (1990), pp. 414–439.
- [39] D Saffar Shamshirgar, Joar Bagge, and A-K Tornberg. “Fast Ewald summation for electrostatic potentials with arbitrary periodicity”. In: *The Journal of Chemical Physics* 154.16 (2021).
- [40] Daria Sushnikova et al. “FMM-LU: A fast direct solver for multiscale boundary integral equations in three dimensions”. In: *Multiscale Modeling & Simulation* 21.4 (2023), pp. 1570–1601.
- [41] Abdunour Y Toukmaji and John A Board Jr. “Ewald summation techniques in perspective: a survey”. In: *Computer physics communications* 95.2-3 (1996), pp. 73–92.
- [42] Xin Xing and Edmond Chow. “Interpolative decomposition via proxy points for kernel matrices”. In: *SIAM Journal on Matrix Analysis and Applications* 41.1 (2020), pp. 221–243.
- [43] Xin Ye, Jianlin Xia, and Lexing Ying. “Analytical low-rank compression via proxy point selection”. In: *SIAM Journal on Matrix Analysis and Applications* 41.3 (2020), pp. 1059–1085.
- [44] Anna Yesypenko. “Randomized algorithms for the efficient solution of elliptic PDEs on modern architectures”. PhD thesis. 2023.
- [45] Anna Yesypenko. *SkelFMM: A Simplified Kernel-Independent Fast Multipole Method in Python*. Version 1.0.0. Jan. 2025. DOI: 10.5281/zenodo.14613533. URL: <https://github.com/annayesy/skelFMM>.
- [46] Anna Yesypenko and Per-Gunnar Martinsson. “Randomized Strong Recursive Skeletonization: Simultaneous Compression and LU Factorization of Hierarchical Matrices using Matrix-Vector Products”. In: *arXiv preprint arXiv:2311.01451* (2023).
- [47] Lexing Ying. “A kernel independent fast multipole algorithm for radial basis functions”. In: *Journal of Computational Physics* 213.2 (2006), pp. 451–457.
- [48] Lexing Ying, George Biros, and Denis Zorin. “A kernel-independent adaptive fast multipole algorithm in two and three dimensions”. In: *Journal of Computational Physics* 196.2 (2004), pp. 591–626.
- [49] Ken-ichi Yoshida, Naoshi Nishimura, and Shoichi Kobayashi. “Application of fast multipole Galerkin boundary integral equation method to elastostatic crack problems in 3D”. In: *International Journal for Numerical Methods in Engineering* 50.3 (2001), pp. 525–547.